2013 21st Mediterranean Conference on Control & Automation (MED)
Platanias-Chania, Crete, Greece, June 25-28, 2013

Preliminary Results on the Estimation Performance of Single Range Source Localization

Pedro Batista, Carlos Silvestre, and Paulo Oliveira

Abstract— **In previous work by the authors a novel estimator was introduced, with asymptotic stability guarantees, for the problems of source localization and navigation based on single range measurements. The aim of this paper is to further study these problems in terms of the performance of the proposed estimators and the trajectories that yield best results. To that purpose, the achievable performance with the proposed estimator is compared with the Bayesian Cramér-Rao Bound (BCRB) for different trajectories of the agent and, in addition, the estimates provided by the Extended Kalman Filter are also computed. It is revealed that the performance of the estimator is close to the BCRB theoretical lower bound and some insight is provided on the effect of the agent trajectory on the estimation performance.**

I. Introduction

The use of range measurements to a single source has been a hot topic of research in the recent past. In [1] a novel algorithm, so-called Synthetic Long Baseline navigation, was proposed for underwater vehicles. In short, a linearized model of the system is obtained and range measurements to a single transponder are employed in order to correct the system estimates, while a high performance dead-reckoning system is used to propagate the motion of the vehicle between range measurements. The problem of underwater navigation based on range measurements to a single beacon is also addressed in [2] considering, in addition, the existence of constant unknown ocean currents. First, the nonlinear system is linearized and the analysis of the observability follows for the linearized system, yielding local results. The proposed estimation solution is the Extended Kalman filter (EKF), with no guarantees of global asymptotic stability. The EKF is, again, the workhorse of the solutions presented in [3] and [4], which address the same problem. The observability of single transponder underwater navigation was studied in [5] resorting to an algebraic approach and algebraic observers were also proposed. The addition of depth measurements to single range readings is considered in [6], where a linearized model is obtained and the EKF is the selected estimation solution. In [7] preliminary experimental results with single beacon acoustic navigation were presented, where the EKF is again employed as the state estimator.

This work was partially supported by the FCT [PEst-OE/EEI/LA0009/2011] and by the EU Project TRIDENT (Contract No. 248497).

The authors are with the Institute for Systems and Robotics, Instituto Superior Técnico, Universidade Técnica de Lisboa, Av. Rovisco Pais, 1049-001 Lisboa, Portugal. Carlos Silvestre is also with the Department of Electrical and Computer Engineering, Faculty of Science and Technology of the University of Macau.

{pbatista,cjs,pjcro}@isr.ist.utl.pt

Parallel to the topic of navigation based on range measurements to a single landmark is the problem of source localization also based on single range measurements. In fact, the problems are equivalent from a theoretical point of view, as detailed in [8]. A novel solution to this problem is proposed in [9], where a localization algorithm based on the square of the range to the source and the inertial position of the agent is detailed, with global exponential stability (GES) guarantees under a persistent excitation condition. The problem of relative pose observability based on range measurements only was addressed in [10] for some specific cases.

In the recent past the authors have proposed a novel solution for the problems of navigation and source localization based on range measurements that achieves globally asymptotically stable error dynamics [8]. In short, the state of the system is first augmented in such a way that the augmented system can be regarded, for observability analysis and observer design purposes, as linear time-varying (LTV). The analysis of observability of the augmented system is then performed and conclusions are afterwards extrapolated to the original nonlinear system. The final result states that an observer for the augmented system is also an observer for the original nonlinear system, and the design follows with a standard Kalman filter. As a result, and in contrast with all the solutions that can be found in the literature that rely on the EKF, this solution guarantees globally asymptotically stable error dynamics provided that the system is uniformly completely observable. Conditions on uniform complete observability are also derived.

While the source localization (and navigation) solution based on single range measurements proposed in [8] offers global asymptotic stability guarantees, the analysis of performance is yet to be performed, which is the main contribution of this paper. To this end, the Bayesian Cramér-Rao Bound (BCRB) is computed for several trajectories and Monte Carlo simulations are performed, with the proposed solution, in order to compare the achieved performance with the BCRB theoretical bound. In addition, Monte Carlo simulations are also carried out, in identical conditions, for the Extended Kalman Filter, which does not offer global asymptotic stability guarantees.

A. Notation

The symbol $\mathbf{0}$ denotes a matrix (or vector) of zeros, $\mathbf{I}$ the identity matrix, and $\mathbf{blkdiag}(\mathbf{A}_1, \ldots, \mathbf{A}_n)$ a block diagonal matrix, all assumed of appropriate dimensions. For $\mathbf{x}, \mathbf{y} \in \mathbb{R}^3$, the cross and inner products are represented by $\mathbf{x} \times \mathbf{y}$

978-1-4799-0995-7/13/$31.00 ©2013 IEEE

and $\mathbf{x}\cdot\mathbf{y}$, respectively. The Dirac delta function is written as $\delta(t)$.

II. Previous work

Consider an agent evolving in a scenario where there is a fixed source. In order to set the problem framework, let $\{I\}$ denote an inertial coordinate reference frame and $\{B\}$ denote the so-called body-fixed reference coordinate frame, which is attached to the agent. In this setting, the kinematics of the agent is given by

$$\begin{cases} \dot{\mathbf{p}}(t) = \mathbf{R}(t)\mathbf{v}_r(t) + \mathbf{R}(t)\mathbf{v}_c(t) \\ \dot{\mathbf{R}}(t) = \mathbf{R}(t)\mathbf{S}\left(\boldsymbol{\omega}(t)\right) \end{cases},$$

where $\mathbf{p}(t)$ denotes the inertial position of the agent, $\mathbf{R}(t)$ is the rotation matrix from $\{B\}$ to $\{I\}$, $\mathbf{v}_r(t)$ is the velocity of the agent relative to the fluid and expressed in body-fixed coordinates, $\mathbf{v}_c(t)$ is the velocity of the fluid relative to $\{I\}$, expressed in body-fixed coordinates, and $\boldsymbol{\omega}(t)$ is the angular velocity of the agent, also expressed in body-fixed coordinates, and $\mathbf{S}\left(\boldsymbol{\omega}\right)$ is the skew-symmetric matrix such that $\mathbf{S}\left(\boldsymbol{\omega}\right)\boldsymbol{x}$ is the cross product $\boldsymbol{\omega}\times\boldsymbol{x}$, for $\boldsymbol{\omega},\boldsymbol{x}\in\mathbb{R}^3$ or, for the problem in 2-D,

$$\mathbf{S}\left(\omega\right) = \begin{bmatrix} 0 & -\omega \\ \omega & 0 \end{bmatrix}.$$

It is assumed that the drift velocity, in inertial coordinates, is constant.

Let $\mathbf{s}$ denote the inertial position of the source and define $\mathbf{r}(t) := \mathbf{R}^T(t)\left[\mathbf{s}-\mathbf{p}(t)\right]$, which corresponds to the position of the source relative to the agent, expressed in body-fixed coordinates, the quantity that is to be estimated in the problem of source localization. The range measurements are simply given by $r(t) = \|\mathbf{r}(t)\|$. As such, the system dynamics for the problem of source localization are given by

$$\begin{cases} \dot{\mathbf{r}}(t) = -\mathbf{S}\left(\boldsymbol{\omega}(t)\right)\mathbf{r}(t) - \mathbf{v}_c(t) - \mathbf{v}_r(t) \\ \dot{\mathbf{v}}_c(t) = -\mathbf{S}\left(\boldsymbol{\omega}(t)\right)\mathbf{v}_c(t) \\ y(t) = \|\mathbf{r}(t)\| \end{cases},$$

where $\mathbf{r}(t)$ and $\mathbf{v}_c(t)$ are the system states, $y(t)$ is the system output, and $\mathbf{v}_r(t)$ and $\boldsymbol{\omega}(t)$ are system inputs.

The estimator proposed in previous work by the authors [8] resorts to the augmentation of the system state, defining the system state as

$$\boldsymbol{x}(t) := \begin{bmatrix} \mathbf{r}^T(t) & \mathbf{v}_c^T(t) & \|\mathbf{r}(t)\| & \mathbf{r}(t)\cdot\mathbf{v}_c(t) & \|\mathbf{v}_c(t)\|^2 \end{bmatrix}^T.$$

In this paper a simpler problem is considered for the sake of easiness of interpretation of results, which consists in assuming that the agent also has access to the velocity relative to the inertial frame. This case also finds many applications in practice, e.g. in ground vehicles with no lateral drift, where a speedometer provides this quantity. In this scenario the augmented state is simply chosen as

$$\boldsymbol{x}_r(t) := \begin{bmatrix} \mathbf{r}(t)^T & y(t) \end{bmatrix}^T$$

and the nonlinear system is given by

$$\begin{cases} \dot{\mathbf{r}}(t) = -\mathbf{S}\left(\boldsymbol{\omega}(t)\right)\mathbf{r}(t) - \mathbf{v}(t) \\ y(t) = \|\mathbf{r}(t)\| \end{cases}. \tag{1}$$

Likewise, the corresponding augmented system is given by

$$\begin{cases} \dot{\boldsymbol{x}}_r(t) = \mathbf{A}_r(t)\boldsymbol{x}_r(t) + \mathbf{B}_r\mathbf{v}(t) \\ y(t) = \mathbf{C}_r\boldsymbol{x}(t) \end{cases}, \tag{2}$$

where

$$\mathbf{A}_r(t) = \begin{bmatrix} -\mathbf{S}\left(\boldsymbol{\omega}(t)\right) & \mathbf{0} \\ -\frac{1}{y(t)}\mathbf{v}^T(t) & 0 \end{bmatrix},$$

$\mathbf{B}_r = \left[-\mathbf{I}\,\mathbf{0}\right]^T$, and $\mathbf{C}_r = \left[\mathbf{0}\,1\right]$. In spite of the fact that this is still a nonlinear system, as the system matrix $\mathbf{A}(t)$ actually depends on the system input and output, it can be regarded as linear time-varying, along trajectories of the system, for observability and observer design purposes, and an estimation solution is readily given by the corresponding Kalman filter, see [8] for further details. This yields an estimation solution with globally asymptotically stable error dynamics, provided that the corresponding observability (and controllability, from system disturbances) conditions are satisfied. In the remainder of the paper this solution is simply called the Kalman filter, in contrast with the EKF.

III. Estimation performance

A. Bayesian Cramér-Rao Bound

The design of estimators for linear systems that minimize appropriate cost functions is well established and prime examples are the Kalman and the $\mathcal{H}_\infty$ filters, see [11] and [12]. For nonlinear systems that is still an open field of research and most results in the design of estimation solutions for nonlinear systems concern the asymptotic stability of the error dynamics. Although definite results on the optimal design of nonlinear estimators are yet to be found, theoretical bounds on the achievable performance have already been derived for some cases.

For time invariant statistical models, the Cramér-Rao Bound (CRB) gives a lower bound on the variance of the estimation error of an unknown constant parameter. For random parameters of nonlinear, non-stationary systems models, an equivalent bound, the Bayesian Cramér-Rao Bound (BCRB), was first derived in [13] and further examined in [14] and [15].

Consider the general system with linear dynamics and nonlinear observations

$$\begin{cases} \dot{\mathbf{x}}(t) = \mathbf{F}(t)\mathbf{x}(t) + \mathbf{B}(t)\mathbf{u}(t) + \mathbf{G}(t)\mathbf{n}_x(t) \\ \mathbf{y}(t) = \mathbf{h}\left(\mathbf{x}(t)\right) + \mathbf{n}_y(t) \end{cases} \tag{3}$$

where $\mathbf{x}(t)$ is the state vector, $\mathbf{u}(t)$ is a deterministic system input, $\mathbf{y}(t)$ is the measurement vector, which depends on the state vector through the nonlinear function $\mathbf{h}\left(\mathbf{x}(t)\right)$, and $\mathbf{n}_x(t)$ and $\mathbf{n}_y(t)$ represent the state and measurements stochastic perturbations, respectively. The Bayesian bound derived in [16] shows that the covariance matrix of any given causal (realizable) unbiased estimate of (3), i.e.

$$E\left\{\left(\mathbf{x}(t)-\hat{\mathbf{x}}(t)\right)\left(\mathbf{x}(\tau)-\hat{\mathbf{x}}(\tau)\right)^T\right\} = \mathbf{P}(t)\delta\left(t-\tau\right),$$

satisfies the lower bound

$$\mathbf{P}(t) \succeq \mathbf{J}_g^{-1}(t), \tag{4}$$

where $\mathbf{J}_g^{-1}(t)$ is the so-called Fisher Information Matrix, which satisfies the matrix differential equation

$$\begin{aligned} \dot{\mathbf{J}}_g(t) &= -\mathbf{J}_g(t)\mathbf{F}(t) - \mathbf{F}^T(t)\mathbf{J}_g(t) \\ &\quad -\mathbf{J}_g(t)\mathbf{G}(t)\boldsymbol{\Xi}(t)\mathbf{G}^T(t)\mathbf{J}_g(t) + \mathbf{P}_m\left(\mathbf{x}(t),t\right), \end{aligned}$$

where $\boldsymbol{\Xi}(t)$ is the covariance matrix of the state noise $\mathbf{n}_x(t)$ and $\mathbf{P}_m\left(\mathbf{x}(t),t\right)$ accounts for the covariance reduction due to the observations, given by

$$\mathbf{P}_m\left(\mathbf{x}(t),t\right) = E_x\left\{\tilde{\mathbf{H}}\left(\mathbf{x}(t)\right)\boldsymbol{\Theta}^{-1}\tilde{\mathbf{H}}^T\left(\mathbf{x}(t)\right)\right\} \tag{5}$$

where $\tilde{\mathbf{H}}(t)$ is the Jacobian of the nonlinear observation function evaluated at $\mathbf{x}(t)$ and $\mathbf{\Theta}(t)$ is the covariance matrix of the measurement noise $\mathbf{n}_y(t)$. The subscript g denotes that the underlying process model is a linear Gaussian model and the subscript m stands for measurement.

The expectation in (5) is computed with respect to the state vector $\mathbf{x}(t)$ and as such it usually has to be evaluated resorting to Monte Carlo simulations. In nonlinear tracking problems, as in the framework presented herein, it is often of interest to evaluate the performance along specific or nominal tracks $\overline{\mathbf{x}}(t)$. In this case, the term $\mathbf{P}_m\left(\mathbf{x}(t), t\right)$ can be simplified to

$$\mathbf{P}_m\left(\overline{\mathbf{x}}(t), t\right) = \tilde{\mathbf{H}}\left(\overline{\mathbf{x}}(t)\right) \mathbf{\Theta}^{-1} \tilde{\mathbf{H}}^T\left(\overline{\mathbf{x}}(t)\right), \tag{6}$$

which allows the assessment of the achievable performance for any tracker or estimator given this specific underlying problem structure. The resulting equations are analogous to the Information filter version of the Extended Kalman Filter, whereas the Jacobians are computed at the nominal trajectories $\overline{\mathbf{x}}(t)$ instead of the estimated trajectories, as convincingly argued in [15].

Notice that, if noise is considered in the angular velocity measurements, the model (3) cannot be applied as there would exist not only additive noise but also multiplicative noise. As (3) does not capture multiplicative noise in the state disturbances, angular velocity noise is not considered in this paper. Future work will include Monte Carlo simulations with angular velocity noise. For the moment, notice that the sole role of this quantity is to explain the rotation of the source, expressed in body-fixed coordinates, when the agent rotates. Hence, it is not directly related to the observability of the system (provided it is available). However, it does influence the estimation performance, in the noisy case, as it influences the confidence in the system dynamics.

Finally, it is important to stress that the BCRB is computed for the original nonlinear system (1), not the augmented state system (2), which are only employed in the estimation solutions.

In this paper, the bound (4) is fundamental to assess the estimation performance of the proposed filters for source localization based on single range measurements. This approach has already been successfully pursued by the authors, in [17], to assess the estimation performance of a navigation system based on an Ultra-Short Baseline acoustic positioning system, whose design corresponds, to a large extent, to the generalization of the design from single to multiple range measurements.

B. Monte Carlo simulations

In order to assess the performance of the proposed Kalman filters, Monte Carlo simulations are carried out and the Root-Mean-Square (RMS) estimation error of the Kalman filter is compared against the BCRB, which is computed for each nominal trajectory that the agent performs. In addition, the performance of the Extended Kalman Filter is also evaluated using the same approach. For the sake of clarity of presentation, only a 2-D case is considered, which is readily obtained by considered an agent moving in the horizontal plane, with all vectors belonging to $\mathbb{R}^2$, scalar angular velocities, and $\mathbf{R}(t) \in SO(1)$. Notice, nevertheless, that the original filtering solution that was proposed solves the problem in 3-D. Moreover, the conclusions drawn for the 2-D case should also yield insight to the 3-D case.

For each scenario, starting at different initial conditions, the filters are evaluated through 1000 Monte Carlo runs and sets of independent random noise. The initial state of the filters is drawn from a normal Gaussian distribution, with mean equal to the true initial state and standard deviation of 10 m and 1 m for the position and the state corresponding to the range, respectively. When the drift velocity is also considered, the standard deviation for the initial ocean current estimate was set to 1 m/s and the standard deviation of the initial estimates of the augmented state estimates $\hat{\mathbf{r}}(t) \cdot \hat{\mathbf{v}}_c(t)$ and $\|\hat{\mathbf{v}}_c(t)\|^2$ was set to 10 m^2/s and 1 m^2/s^2, respectively. The reasoning for setting the initial estimates around the true value is that the purpose of the paper is to assess the performance and convergence in terms of error covariance, not the convergence in nominal terms, which has already been successfully established for the proposed application of the Kalman filter, see [8], and that is still absent, to the best of the authors' knowledge, for the EKF. Common to all the simulations is the inclusion of additive, zero-mean white Gaussian noise, with standard deviation of 1 m for the range measurements and 0.01 m/s for the relative velocity measurements.

First, the case without drift (1) is considered. To tune the Kalman filter for (2), the state disturbance intensity matrix is chosen as $\mathbf{\Xi}_r = \textbf{blkdiag}\left(0.01^2\mathbf{I}, 0.001^2\right)$ which reflects the noise of the velocity sensor, while the output noise intensity matrix is chosen as $\mathbf{\Theta} = \mathbf{I}$, which reflects the noise of the range sensor. For the EKF the state disturbance intensity matrix is simply $0.01^2\mathbf{I}$ and the output noise intensity matrix is the same of the Kalman filter.

The first trajectory that is considered is depicted in Fig. 1, where the use of color is employed in order to reflect the time evolution: the agent position is initially depicted in dark blue and progressively changes to dark red, passing through shades of cyan, green, yellow, and orange, in this order. In this trajectory the x-axis of the agent is always tangent to the path, which means that the angular velocity is non-null. This first case study will henceforth be denoted as case A. The trajectory is quite rich, ensuring observability, and the agent is operating in the vicinity of the source, which is marked with a red cross in the figure. The evolution of the statistical variables that were computed with Monte Carlo simulations, as well as the Bayesian Cramér-Rao Bound, are depicted in Fig. 2. In particular, for each time instant, the average of the error of both the Kalman filter and the Extended Kalman filter is computed and shown in Fig. 2(a). In Fig. 2(b) the information regarding the second order statistical moments is depicted: i) the Bayesian Cramér-Rao Bound, in green; ii) the Root-Mean-Square (RMS) of the errors of the Kalman filter, computed for each instant, in blue; iii) the square root of the first two diagonal elements of the covariance matrix of the Kalman filter, in red; iv) the RMS of the errors of the EKF, computed for each instant, in magenta; and v) the square root of the diagonal elements of the covariance matrix

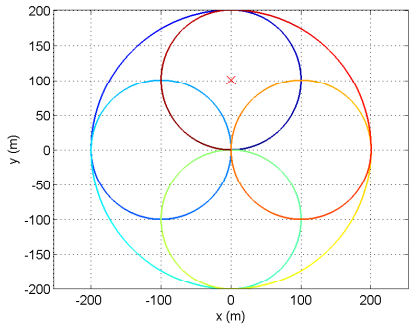

Fig. 1. Evolution of the trajectory of the agent - case study A

of the EKF, in yellow. From these first plots it is possible to

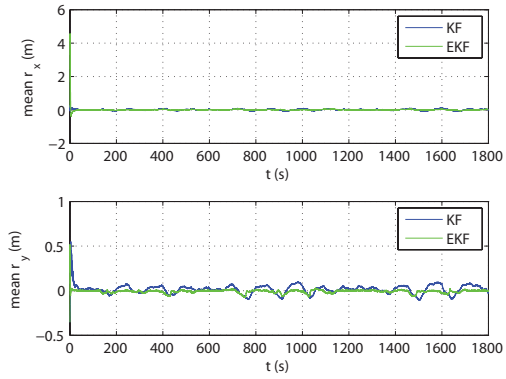

(a) Mean error

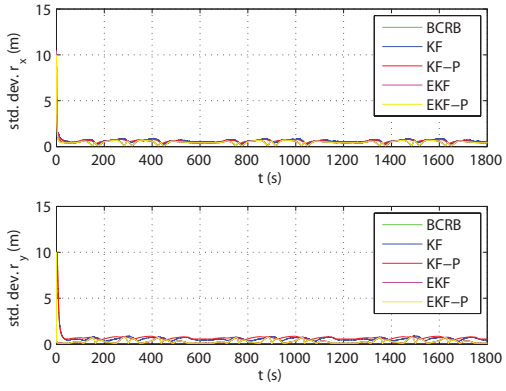

(b) Standard deviation

Fig. 2. Evolution of statistical variables - case study A

observe that: i) the mean error stays close to zero for both filters; ii) the covariance of the EKF filter agrees with the BCRB and the RMS of the EKF follows this very closely; and iii) the RMS error of the Kalman filter follows closely the square root of the corresponding Kalman filter covariance matrix elements; and iv) the performance of the Kalman filter is close to the BCRB. In Fig. 3 the norm of the statistical variables is depicted considering each as a 2-D vector, e.g. if $\mathrm{BCRB_x(t)}$ corresponds to the BCRB for the error of $r_x(t)$ and $\mathrm{BCRB_y(t)}$ corresponds to the BCRB for the error of $r_y(t)$, the norm would be $\sqrt{\mathrm{BCRB_x^2(t)} + \mathrm{BCRB_y^2(t)}}$. It is

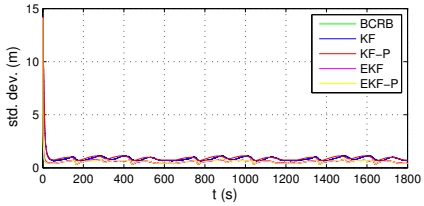

Fig. 3. Evolution of the norm of the statistical variables - case study A

possible to observe that all the signals are close to the BCRB.

Next, simulations were carried out with a similar trajectory but obtained with no angular velocity, which was achieved by changing the input linear velocity. This scenario will be henceforth denoted as case study B. In this case, no significant changes are noticeable and the performance of the Kalman filter is, again, close to the BCRB. The evolution of the statistical variables is roughly the same and as such it is omitted.

Next, the same trajectory is considered but the source is positioned farther away from the agent, with $\mathbf{s} = [0\,2000]$ m. In the first set of simulations for this case the agent has, once again, angular velocity, so that the x-axis of the agent is always tangent to the path. This case study will be henceforth denoted as case study C. The statistical information, as well as the BCRB, are depicted in Fig. 4 and relevant changes are visible. First, the RMS error of the EKF, which follows closely the square root of the diagonal elements of its covariance matrix, which agree with the BCRB, exhibits oscillations in both axes. Next, these quantities are below, for most of the time, the RMS of the Kalman filter, which follows closely the square root of the diagonal elements of the Kalman filter covariance matrix. In Fig. 5 the norm of the statistical variables is depicted. In spite of the frequent oscillations in each component, it is now possible to observe that the norm fluctuates little. Moreover, it is more evident that the Kalman filter does not achieve the same level of performance. In fact, the norm of the statistical variables for the Kalman filter, in steady-state, corresponds roughly to that for the EKF (or the BCRB) times $\sqrt{2}$. More on this will be discussed shortly. Also, from the comparison of Figs. 5 and 3 it is possible to conclude that the increase of the distance from the agent to the source led to a decrease in terms of performance.

The case study C was modified, in such a way that, again, the agent has no angular velocity but the trajectory remains the same. This case is henceforth denoted as case study D and the corresponding statistical variables are depicted in Fig. 6. In comparison with Fig. 4, it is readily clear that the oscillations vanish almost completely. Moreover, the evolution of the norm is roughly the same as of Fig. 5 and as such it is omitted. These observations suggest, as expected, that the angular velocity of the agent, in the absence of angular velocity noise, plays no role in the estimation performance. In fact, in these conditions, a simple rotation of the agent, without displacement, simply moves the uncertainty of the estimate of the position of the source from one axis to the other. Another distinct feature of Fig. 6

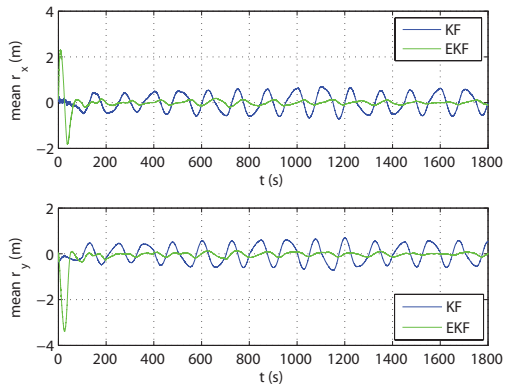

(a) Mean error

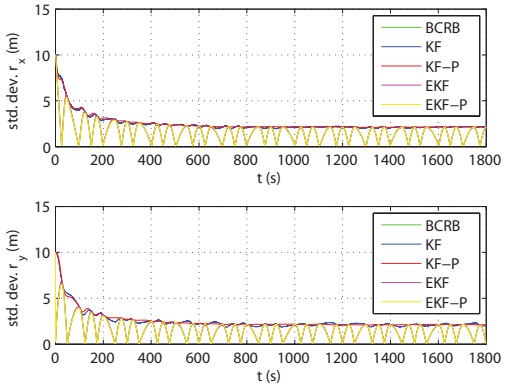

(b) Standard deviation

Fig. 4. Evolution of statistical variables - case study C

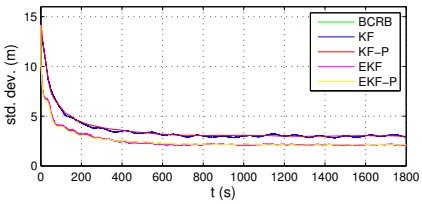

Fig. 5. Evolution of the norm of the statistical variables - case study C

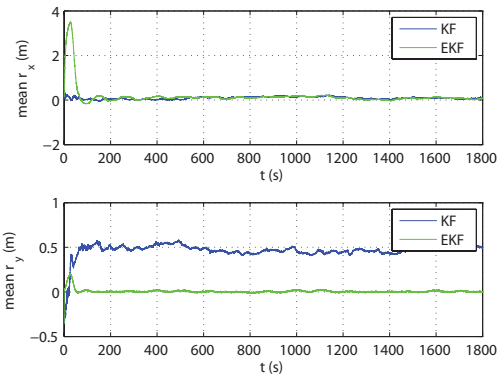

(a) Mean error

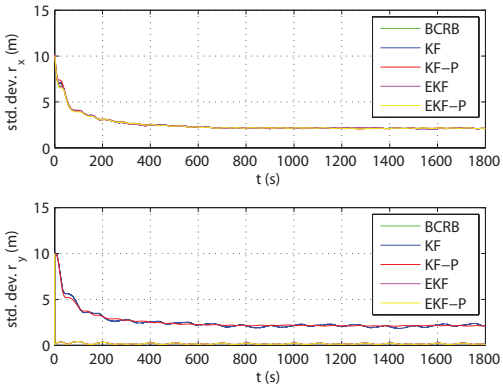

(b) Standard deviation

Fig. 6. Evolution of statistical variables - case study D

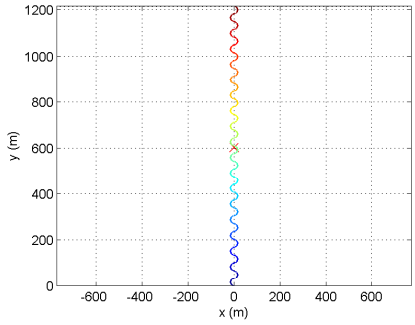

Fig. 7. Evolution of the trajectory of the agent - case study E

is that, while on the x-axis the performance of the Kalman filter is equivalent to that of the EKF (and is tight to the BCRB), the same does not happen for the y-axis. In fact, the Kalman filter has about the same performance on both axes, and hence the norm of this quantity is roughly that of the EKF times $\sqrt{2}$. This also happens in Fig. 3. Notice also that the Kalman filter suffers a little bit more in terms of the mean error, in both case studies C and D, in which the distance from the agent to the source is larger.

In case studied E the agent follows a substantially different trajectory, as depicted in Fig. 7. This trajectory is less rich and a lot closer to a straight line, which would render the system unobservable, leading to the divergence of the filters and the BCRB. In this case the trajectory was achieved without angular velocity in order to better analyze the estimation results. The statistical information obtained with Monte Carlo simulations, as well as the BCRB, are depicted in Fig. 8. Along the y-axis all the statistical variables are tight to the BCRB and the mean error of both filters is very close to zero, with slightly higher transients for the EKF. While the performance of the EKF is also tight to the BCRB along the x-axis, with mean close to zero, the Kalman filter suffers along this axis: in short, it achieves roughly the same performance as along the y-axis, adding the mean to the RMS error. Another noticeable feature is that the performance increases as the agent approaches the source and decreases as it moves away from it. All these conclusions are in line with previous observations.

Finally, circular trajectories around the source were considered and some of the conclusions drawn before were again observed. For instance, even with a non-null angular

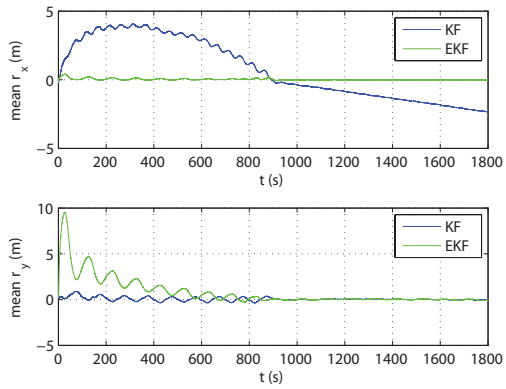

(a) Mean error

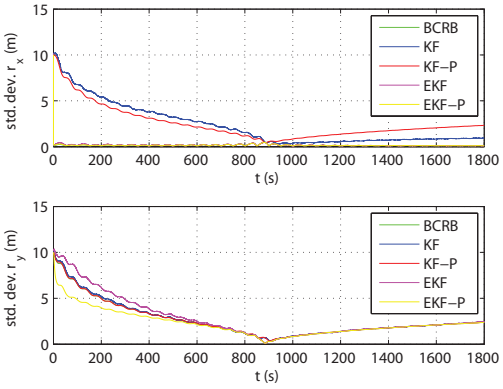

(b) Standard deviation

Fig. 8. Evolution of statistical variables - case study E

velocity, there are no oscillations as long as the direction of the source is constant in body-fixed coordinates, hence leading to no shift in uncertainty between axes. However, the direction of the source is not constant in inertial coordinates, which renders the system observable in this case. Another interesting observation was that the speed at which the same path was followed impacts the performance. In particular, faster velocities lead to an improvement of the estimation performance. This is in line with the observation term (6), which in this case is given by

$$\mathbf{P}_m\left(\overline{\mathbf{x}}(t),t\right) = \overline{\mathbf{d}}(t)^T \boldsymbol{\Theta} \overline{\mathbf{d}}(t),$$

where $\overline{\mathbf{d}}(t) = \overline{\mathbf{r}}(t)/\left\|\overline{\mathbf{r}}(t)\right\|$ is the nominal direction of the source relative to the agent.

IV. Conclusions

This paper presented the analysis of the estimation performance of a filtering solution with globally asymptotically stable error dynamics for the problem of source localization based on single range measurements. Several trajectories were considered, the performance of the Extended Kalman filter was also assessed, and both solutions were matched against the Bayesian Cramér-Rao Bound. In short, the performance of the EKF is tight to the BCRB, though GAS error dynamics are yet to be established. In contrast, the performance of the proposed solution is tight to the BCRB in one direction but lags in the orthogonal one - it achieves only the same performance as in the other direction, while the BCRB is lower. This seems to be the price of the state augmentation technique, in this case, that yields, nevertheless, globally asymptotically stable error dynamics. The estimation performance is related to the evolution of the direction of the source, expressed in inertial coordinates, while changes of this vector expressed in body-fixed coordinates simply redistribute the uncertainty of the estimates among the axes of the agent. Finally, the distance from the source to the agent does not seem to affect, per se, the estimation performance, which is related to the evolution of the direction of the source to the agent, as hinted by the Jacobian of the observations.

References

[1] M. Larsen, "Synthetic long baseline navigation of underwater vehicles," in *Proceedings of the 2000 MTS/IEEE Oceans*, vol. 3, Providence, RI, USA, Sep. 2000, pp. 2043–2050.

[2] A. Gadre and D. Stilwell, "A complete solution to underwater navigation in the presence of unknown currents based on range measurements from a single location," in *Proceedings of the 2005 IEEE/RSJ International Conference on Intelligent Robots and Systems*, Edmonton AB, Canada, Aug. 2005, pp. 1420–1425.

[3] T. Casey, B. Guimond, and J. Hu, "Underwater Vehicle Positioning Based on Time of Arrival Measurements from a Single Beacon," in *Proceedings of the MTS/IEEE Oceans 2007*, Vancouver, BC, Canada, Sept.-Oct. 2007, pp. 1–8.

[4] P.-M. Lee, B.-H. Jun, K. Kim, J. Lee, T. Aoki, and T. Hyakudome, "Simulation of an Inertial Acoustic Navigation System With Range Aiding for an Autonomous Underwater Vehicle," *IEEE Journal of Oceanic Engineering*, vol. 32, no. 2, pp. 327–345, Apr. 2007.

[5] J. Jouffroy and J. Reger, "An algebraic perspective to single-transponder underwater navigation," in *Proceedings of the 2006 IEEE International Conference on Control Applications*, Munich, Germany,, Oct. 2006, pp. 1789–1794.

[6] G. Antonelli, F. Arrichiello, S. Chiaverini, and G. Sukhatme, "Observability analysis of relative localization for AUVs based on ranging and depth measurements," in *Proceedings of the 2010 IEEE International Conference on Robotics and Automation*, Anchorage, Alaska, USA, May 2010, pp. 4286–4271.

[7] S. Webster, R. Eustice, H. Singh, and L. Whitcomb, "Preliminary deep water results in single-beacon one-way-travel-time acoustic navigation for underwater vehicles," in *Proceedings of the 2009 IEEE/RSJ International Conference on Intelligent Robots and Systems- IROS 2009*, SaintLouis, MO, USA, Oct. 2009, pp. 2053–2060.

[8] P. Batista, C. Silvestre, and P. Oliveira, "Single Range Aided Navigation and Source Localization: observability and filter design," *Systems & Control Letters*, vol. 60, no. 8, pp. 665–673, Aug. 2011.

[9] B. Fidan, S. Dandach, S. Dasgupta, and B. Anderson, "A continuous time linear adaptive source localization algorithm robust to persistent drift," *Systems & Control Letters*, vol. 58, no. 1, pp. 7–16, Jan. 2009.

[10] G. Parlangeli, P. Pedone, and G. Indiveri, "Relative Pose Observability Analysis for 3D Nonholonomic Vehicles Based on Range Measurements Only," in *Proceedings of the 9th IFAC Conference on Manoeuvring and Control of Marine Craft*, Arenzano, Italy, Sep. 2012, pp. 1–6.

[11] A. Gelb, *Applied Optimal Filtering*. The MIT Press, 1974.

[12] K. Nagpal and P. Khargonekar, "Filtering and Smoothing in an $\mathcal{H}_\infty$ Setting," *IEEE Transactions on Automatic Control*, vol. 36, no. 2, pp. 152–166, Feb. 1991.

[13] H. van Trees, "Bounds on the accuracy attainable in the estimation of continuous random processes," *IEEE Transactions on Information Theory*, vol. 12, no. 3, pp. 298 – 305, Jul. 1966.

[14] ——, *Detection, Estimation, and Modulation Theory. Part I: Detection, Estimation, and Linear Modulation Theory (Part 1)*. John Wiley & Sons, 1968.

[15] ——, *Bayesian Bounds for Parameter Estimation and Nonlinear Filtering/Tracking*. Wiley-IEEE Press, 2007.

[16] D. Snyder and I. Rhode, "Filtering and control performance bounds with implications on asymptotic separation," *Automatica*, vol. 8, no. 6, pp. 747–753, Nov. 1972.

[17] M. Morgado, P. Batista, P. Oliveira, and C. Silvestre, "Position USBL/DVLSensor-based Navigation Filter in the presence of Unknown Ocean Currents," *Automatica*, vol. 47, no. 12, pp. 2604–2614, Dec. 2011.